Near-Unitary Spin Squeezing in ^{171}Yb (Supplemental Material)

Boris Braverman,[1] Akio Kawasaki,[1] Edwin Pedrozo-Peñafiel,[1] Simone Colombo,[1] Chi Shu,[1, 2] Zeyang Li,[1] Enrique Mendez,[1] Megan Yamoah,[1] Leonardo Salvi,[1, 3] Daisuke Akamatsu,[1, 4] Yanhong Xiao,[1, 5] and Vladan Vuletić[1]

[1]*Department of Physics, MIT-Harvard Center for Ultracold Atoms and Research Laboratory of Electronics,*
Massachusetts Institute of Technology, Cambridge, Massachusetts 02139, USA
[2]*Department of Physics, Harvard University, Cambridge, Massachusetts 02138, USA*
[3]*Dipartimento di Fisica e Astronomia and LENS - Università di Firenze,*
INFN - Sezione di Firenze, Via Sansone 1, 50019 Sesto Fiorentino, Italy
[4]*National Metrology Institute of Japan (NMIJ), National Institute of Advanced Industrial Science and Technology (AIST),*
1-1-1 Umezono, Tsukuba, Ibaraki 305-8563, Japan
[5]*Department of Physics, State Key Laboratory of Surface Physics and Key Laboratory of Micro and*
Nano Photonic Structures (Ministry of Education), Fudan University, Shanghai 200433, China

I. TECHNICAL AND EXPERIMENTAL DETAILS

Cold ^{171}Yb atoms are prepared in a two-color magneto-optical trap (MOT) [1] and then cooled further in a single-color MOT on the triplet transition $^1S_0 \rightarrow ^3P_1$ with wavelength λ=556 nm and linewidth $\Gamma/(2\pi)$=184 kHz. The atoms are transported into an asymmetric high-finesse optical cavity [2] by adjusting the magnetic field of the MOT, and loaded into a one-dimensional optical lattice with wavelength λ_t=759 nm and trap depth U_0=$k_B \times$120 μK. In order to remove hot atoms with weaker coupling to the cavity mode, the trap depth is lowered to $U_0/3$ and restored to U_0 over 85 ms. The temperature of the remaining $N_{\rm tot}\approx$1500 atoms is T=(20±5) μK.

The asymmetric cavity consists of a large spherical mirror with radius of curvature R_1=25 mm, and a slightly elliptical micromirror with an average radius R_2=344 μm [2]. The cavity finesse is $\mathcal{F}$=1.2×10^4 at the probe wavelength λ, corresponding to a cavity linewidth $\kappa/(2\pi)$=520 kHz. The single-atom cooperativity at an antinode is given by η_0=24$\mathcal{F}/(\pi k^2 w^2)$ [3]. At a distance of 0.42 mm from the micromirror, the probe mode waist is $w = 15.1$ μm, giving η_0=2.4, which means that the system is in the strong-coupling regime [4–6] (see also Ref. [2] for details). Since $\lambda \neq \lambda_t$, the atoms are inhomogeneously coupled to the probe. As in Refs. [7, 8], we define an effective atom number N=$N_{tot}\langle\eta\rangle^2/\langle\eta^2\rangle$=$\frac{2}{3}N_{tot}$ and effective single-atom cooperativity η=$\langle\eta^2\rangle/\langle\eta\rangle$=$\frac{3}{4}\eta_0$, so that the spin projection noise, measured via the cavity, satisfies the usual relation $(\Delta N)^2$=$N/4$ for a CSS. The experiments described below are performed with $N\approx$1000, η=1.8(1), and a collective cooperativity $N\eta\approx$1800. The effective cooperativity η is confirmed in an independent measurement (see III).

We perform squeezing between the nuclear sublevels $|\uparrow\rangle \equiv \left|m_I=\frac{1}{2}\right\rangle$ and $|\downarrow\rangle \equiv \left|m_I=-\frac{1}{2}\right\rangle$ of the electronic $^1S_0$ ground state of ^{171}Yb. The collective spin state can be represented on a Bloch sphere with radius S=$N/2$ [8]. The cavity frequency ω_c is tuned to be nearly resonant ($\omega_c-\omega_a$=$2\pi \times -340$ kHz) with the $|\uparrow\rangle \rightarrow \left|^3P_1, m_F = \frac{3}{2}\right\rangle$ atomic transition with frequency ω_a in the presence of a magnetic field B_z=13.6 G along the cavity axis. $N_\uparrow$ atoms in the state $|\uparrow\rangle$ induce a vacuum Rabi splitting $2g$=$\sqrt{N_\uparrow \eta \kappa \Gamma}$ of the cavity resonance (Fig. S2). Near the equator of the Bloch sphere, where $N_\downarrow \approx N_\uparrow$, there is also a small dispersive effect from the $N_\downarrow$ atoms in the state $|\downarrow\rangle$, suppressed by the Zeeman splitting Δ_z=$2\pi \times 18.5$ MHz between magnetic sublevels in the excited $^3P_1$ state, with $\Delta_z\gg\Gamma,\kappa$. To accurately analyze the experiments described below, we need to consider both the near-resonant transition $|\uparrow\rangle \rightarrow \left|^3P_1, m_F = \frac{3}{2}\right\rangle$ and the detuned transition $|\downarrow\rangle \rightarrow \left|^3P_1, m_F = \frac{1}{2}\right\rangle$.

S_z is determined by detecting $N_\uparrow$ via a measurement of the Rabi splitting $2g$, swapping the populations of $|\uparrow\rangle$ and $|\downarrow\rangle$ with a radiofrequency π pulse, and remeasuring the Rabi splitting to give $N_\downarrow$. From $N_\uparrow$ and $N_\downarrow$, we determine $S_z = (N_\uparrow - N_\downarrow)/2$, and $S = (N_\uparrow + N_\downarrow)/2$ using the two-transition atomic model and the separately measured cavity parameters (III). The primary quantity of interest, denoted by $\sigma^2 \equiv 2\,(\Delta S_z)^2/S$, is the spin variance $(\Delta S_z)^2$ normalized to the CSS noise $(\Delta S_z)^2_{CSS} = S/2$. The SQL corresponds to σ^2=1. Our experimental cavity is frequency-stabilized to the trap laser λ_t=759 nm, whose frequency is stabilized to a stable external reference cavity. The bridging frequency between this cavity and the experimental cavity is set through a sideband generated by an electro-optic modulator (EOM). We use the Pound-Drever-Hall technique to lock the cavity to the trap light. In order to actively suppress slow drifts of the experimental cavity resonance frequency with respect to the atomic transition we scan the probe light (λ=556 nm), which is locked to an ultra-stable cavity, and monitor the transmission of the probe light through the cavity. With this we can precisely determine the resonance frequency of the experimental cavity relative to the ultra-stable cavity. We keep this frequency stable from run to run by feeding back through an FPGA circuit on the bridging frequency with an error of less than 15 kHz.

II. MEASUREMENT OF THE ATOMIC STATE

The collective atomic state projection S_z is obtained from the difference $S_z=(N_\uparrow - N_\downarrow)/2$ between the two populations $N_\uparrow$ and $N_\downarrow$ of the states $|\uparrow\rangle = \left|6s^2\ ^1S_0,\ m_I = \frac{1}{2}\right\rangle$ and $|\downarrow\rangle = \left|6s^2\ ^1S_0,\ m_I = -\frac{1}{2}\right\rangle$. We first measure the population $N_\uparrow$ of the $|\uparrow\rangle$ state through the vacuum Rabi splitting of the cavity mode $2g\approx\sqrt{N_\uparrow\eta\kappa\Gamma}$ occurring when the empty cavity mode frequency ω_c is resonant with the atomic transition $|\uparrow\rangle \rightarrow \left|^3P_1, m_F = \frac{3}{2}\right\rangle$ with frequency ω_a. After that, we apply a radiofrequency (RF) π-pulse that switches the populations of $|\uparrow\rangle$ and $|\downarrow\rangle$, and remeasure the Rabi splitting which is now proportional to $\sqrt{N_\downarrow}$. We implement the following state measurement sequence $(N_\uparrow^{(1a)}-N_\downarrow^{(1a)}-N_\downarrow^{(1b)}-N_\uparrow^{(1b)}-N_\uparrow^{(2a)}-N_\downarrow^{(2a)}-N_\downarrow^{(2b)}-N_\uparrow^{(2b)})$. The inferred S_z values for the two measurements ($i = 1, 2$) are $S_z^{(i)}=(N_\uparrow^{(ia)} + N_\uparrow^{(ib)} - N_\downarrow^{(ia)} - N_\downarrow^{(ib)})/4$. We define the quality of a single measurement as the normalized variance $\sigma_d^2 \equiv \mathrm{var}\left(S_z^{(2)} - S_z^{(1)}\right)/S$.

In principle, to determine the state S_z it is sufficient to measure $N_\uparrow$, apply a $\pi-$pulse, and measure $N_\downarrow$. However, in this way the two populations are not measured simultaneously, resulting in additional noise due to atom number decay. By measuring $N_\downarrow$ and $N_\uparrow$ twice, as described in the previous paragraph, we can eliminate the noise due to atom decay to first order.
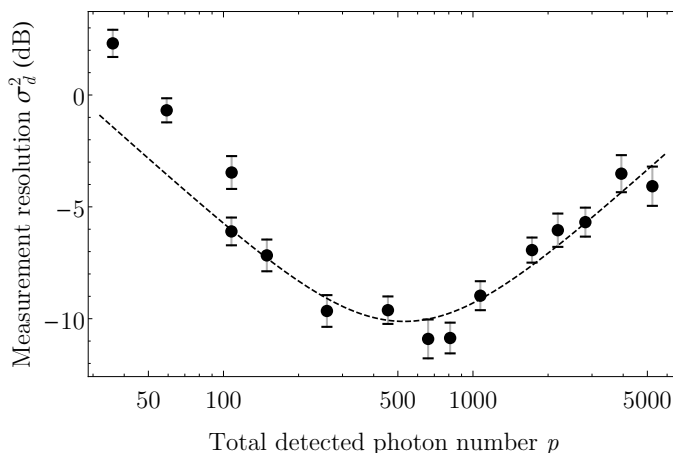

FIG. S1: Variance of the difference between two repeated measurements on the same spin state, normalized to the SQL, vs. total detected photon number p per measurement. For small photon number, the measurement quality increases proportionately to p. However, at large photon number the variance increases again due to Raman scattering. The dashed line is a fit of form $\sigma_d^2 = a/p + bp$ with $a=26(9)$ and $b=9.2(8)\times10^{-5}$. The parameters for these measurements are $N\sim1000$, $\eta=2.0(3)$.

Note that because of the existence of the second (detuned) transition $|\downarrow\rangle \rightarrow \left|^3P_1, m_F = \frac{1}{2}\right\rangle$, the vacuum Rabi peaks are not exactly symmetric, and we detune the cavity by a small amount $\omega_c - \omega_a = -2\pi \times 340$ kHz from the atomic frequency to cancel the asymmetry to lowest order. We use the exact relation $2g(N_\uparrow, N_\downarrow)$ when determining the populations from the measured Rabi splittings.

In Fig. S2 it is shown the Rabi splitting measurement performed by simultaneously sending two laser sidebands, at $\omega_c\pm\omega_m$, into the atom-cavity system. In this way, we can detect both vacuum Rabi peaks simultaneously, while being robust against laser and cavity noise. We perform a linear chirp of the modulation frequency ω_m from 0 to 7 MHz in 10 ms, and detect the transmitted light that contains a beat note at $2\omega_m$. Information about the atomic state is contained in both the intensity and the phase of the signal at $2\omega_m$. We record the arrival times of the transmitted photons and fit both the intensity and phase; using the phase information in addition to the intensity improves the detection by up to a factor of 4.

As shown in Fig. S1, detection of more photons improves the S_z detection until Raman scattering increases the S_z noise [9–13]. In our system, Raman scattering is suppressed to 5% of Rayleigh scattering due to the small atomic linewidth $\Gamma = 2\pi \times 184$ kHz and Rabi splitting $g \approx 2\pi \times 4$ MHz compared to the Zeeman splitting $\Delta_z = 2\pi \times 18.5$ MHz. This enables reasonably good detection at our relatively small atom number $N\approx10^3$ compared to $N = 5 \times 10^5$ atoms as used in Refs. [10, 11] which have demonstrated record squeezing. However, our detection is 4 dB worse than the optimum expected for our photon detection efficiency of 15%. This is likely caused by the imperfect contrast in the chirp measurement, which hinders the possibility of using the entire phase information acquired in the heterodyne detection.
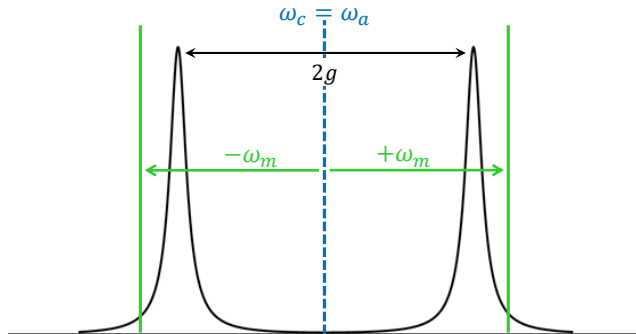
FIG. S2: Sketch of the implemented heterodyne measurement. Two laser sidebands (green solid vertical lines) are simultaneously chirped from the frequency of the empty cavity mode (blue dashed vertical light) through the blue and red detuned Rabi peaks, respectively. We use the beating between these two sidebands (beat note at $2\omega_m$) to measure the Rabi splitting $2g$.

III. MEASUREMENT OF SINGLE-ATOM COOPERATIVITY η AND DETERMINATION OF STANDARD QUANTUM LIMIT (SQL)

The single-atom cooperativity η can be calculated from the cavity parameters and the measured position of the atoms along the cavity mode. It can also be experimentally verified from the spin noise, measured via the cavity, as a function of collective cooperativity $N\eta$ [9]. For a state prepared at the equator of the Bloch sphere, the variance of the difference $S_z\eta=(N_\uparrow - N_\downarrow)\eta/2$ at the projection noise limit (standard quantum limit (SQL)) is given by

$$\mathrm{var}\left(\frac{N_\uparrow\eta - N_\downarrow\eta}{2}\right) = (N_\uparrow+N_\downarrow)\frac{\eta^2}{4}=(N\eta)\frac{\eta}{4}, \tag{S1}$$

where $N = N_\uparrow + N_\downarrow=N_{tot}\langle\eta\rangle^2/\langle\eta^2\rangle$ is the effective atom number, and $\eta = \langle\eta^2\rangle/\langle\eta\rangle$ the effective cooperativity. For atoms uniformly (or randomly) distributed along the length of the cavity, we have $N = \frac{2}{3}N_{tot}$ and $\eta = \frac{3}{4}\eta_0$ [8]. Here, N_{tot} is the actual number of atoms coupled to the cavity, while η_0 is the cooperativity at a cavity antinode, given by

$$\eta_0 = \frac{24\mathcal{F}}{\pi k^2 w^2} \tag{S2}$$

for a Gaussian cavity mode. In (S2), $\mathcal{F}$ is the cavity finesse, $k = 2\pi/\lambda$ is the wavevector of light resonant with the atomic transition, and w is the $1/e^2$ intensity radius of the cavity mode at the position of the atoms. The asymmetric structure of our optical cavity makes the mode waist w position-dependent [2], and equal to $w = 15.1\,\mu$m at the distance of 0.42 mm from the micromirror where we trap the atoms for all experiments described here.

Plotting the measured variance of $\frac{1}{2}(N_\uparrow\eta - N_\downarrow\eta)$ as a function of the measured total cooperativity $N\eta$ yields $\eta/4$ as the slope of the line, as shown in Fig. S3. The result, η=1.8(1), agrees with the expected value $\eta = 1.8(2)$ calculated from the cavity parameters and first principles [3]. The SQL in the population difference quadrature is then given by $(\Delta S_z)^2 =S/2=N/4$. The linear dependence in Fig. S3 demonstrates that our system is dominated by quantum noise. We fitted the data also to a quadratic model (see Fig. S3) obtaining η=1.6(2), which equally agrees with the expected cooperativity. However, the $p-$value of the estimated quadratic coefficient is 0.28, which means that such a coefficient is consistent with 0. We thus use the simple linear fit as the best estimator of η.

IV. GENERATION OF RF PULSES

To drive the transition between the two magnetic sublevels $m_I=\pm\frac{1}{2}$ of the ground state $\left|{}^1S_0, I = \frac{1}{2}\right\rangle$ of ^{171}Yb we use radiofrequency (RF) pulses. The nuclear g factor of ^{171}Yb is equal to $g_I = -0.4919(3)$, resulting in a Zeeman shift of $\Delta_{z,I}(m_I) = g_I\mu_N m_I = 2\pi \times -375\,$Hz/G $\times m_I$. Thus, the transition frequency $\left|m_I=\frac{1}{2}\right\rangle \to \left|m_I= -\frac{1}{2}\right\rangle$ has a Zeeman shift of $\Delta_{z,I}(\frac{1}{2}) - \Delta_{z,I}(-\frac{1}{2})$=$2\pi \times -750\,$Hz/G. At a typical applied field of B_z=13.6 G, the resulting splitting (Larmor frequency) is $2\pi \times 10.2\,$kHz. The RF-pluses necessary to drive nuclear spin flips are generated using a single coil which is composed of two independent conductors, generating an oscillating magnetic field in the $\hat{x}$ direction. Each conductor carries the same AC current, but opposite DC currents, to avoid altering the DC magnetic field
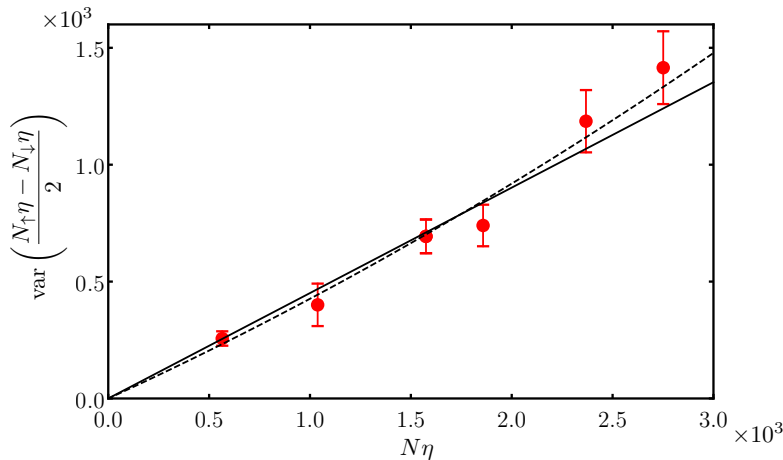
FIG. S3: Determination of the effective cooperativity from measured spin noise, see Eq. (S1). The solid line represents the data fitted to a linear model, while for the dashed line the model is quadratic.

experienced by the atoms. With an amplitude of 63 A for the alternating current, a Rabi frequency of 208(2) Hz is obtained. More details about the configuration and control of the magnetic field for Rabi pulses can be found in [14].

In order to be insensitive to the environmental magnetic field variations, we use a CORPSE composite π-pulse [15, 16] in the spin echo sequence. We perform the spin-echo pulse around the S_x axis, i.e., the direction of the average spin vector. The CORPSE pulse consists of the following three pulses [15, 16]:

$$\left[\theta_1\right]_{[\phi_1]}\left[\theta_2\right]_{[\phi_2]}\left[\theta_3\right]_{[\phi_3]} \tag{S3}$$

In this equation, θ_i is the pulse area and ϕ_i is the relative phase. We choose $\theta_1=2\pi + \theta/2 - k$, $\theta_2 = 2\pi - 2k$, and $\theta_3=\theta/2 - k$, with $k = \arcsin[\sin(\theta/2)/2]$, and θ is the target rotation pulse area, which in our case is $\theta=\pi$. The phases of the three pulses are given by $\phi_1 = \phi_2 - \pi=\phi_3=\phi$, where ϕ is the phase of the composite pulse. The lengths of the pulses are 5.25 ms, 3.75 ms, and 0.75 ms, respectively. The pulse areas are calibrated by Rabi spectroscopy between the nuclear sublevels $m_I = \pm\frac{1}{2}$. The simple π Rabi pulse has an efficiency of 98%. For calibration of the Larmor frequency, we perform Ramsey spectroscopy in the space of the nuclear spin states, with Ramsey times ranging from 1 ms to 50 ms.

V. EXPERIMENTAL SEQUENCE FOR TWO-COLOR SQUEEZING

Figure S4 shows the detailed experimental sequence, a condensed version of which is shown in Fig. 1(d) of the main text. Optical pumping puts all atoms into the $|\uparrow\rangle$ state. A $\pi/2$ pulse (see Sec. IV) prepares a coherent spin state (CSS) along the $+\hat{x}$ direction. Two squeezing pulses are sequentially sent into the cavity, with frequencies $\omega_{l1} = \omega_a+2\pi\times7.33$ MHz and $\omega_{l2} = \omega_a-2\pi\times2.00$ MHz respectively, and a relative incident power ratio of $P_2/P_1=0.53$. The shearing induced by a photon at ω_{l2} is greater than for a photon at ω_{l1} due to a smaller detuning from atomic resonance.

At this point, a SSS is already produced, but an N-dependent first-order phase shift has displaced the state away from pointing in the $+\hat{x}$ direction. To compensate for this shift, we perform a spin echo sequence, by applying a CORPSE π pulse around the $+\hat{y}$ direction, and sending two more squeezing pulses through the cavity, now in reverse order: ω_{l2} followed by ω_{l1}, with the same power ratio as before. The spin echo sequence also cancels spin dephasing due to inhomogeneous magnetic fields. The final step in the sequence is a rotation of the state around the $+\hat{x}$ direction by a variable angle α, followed by the state detection sequence described in Section II.

VI. COMPENSATION FOR FLUCTUATIONS IN THE TOTAL ATOM NUMBER

For an initial CSS near the Bloch sphere equator (fixed $S_z \approx 0$), fluctuations in the total atom number N change the vacuum Rabi splitting and the shearing strength Q per incident photon. If the atom number N is greater,
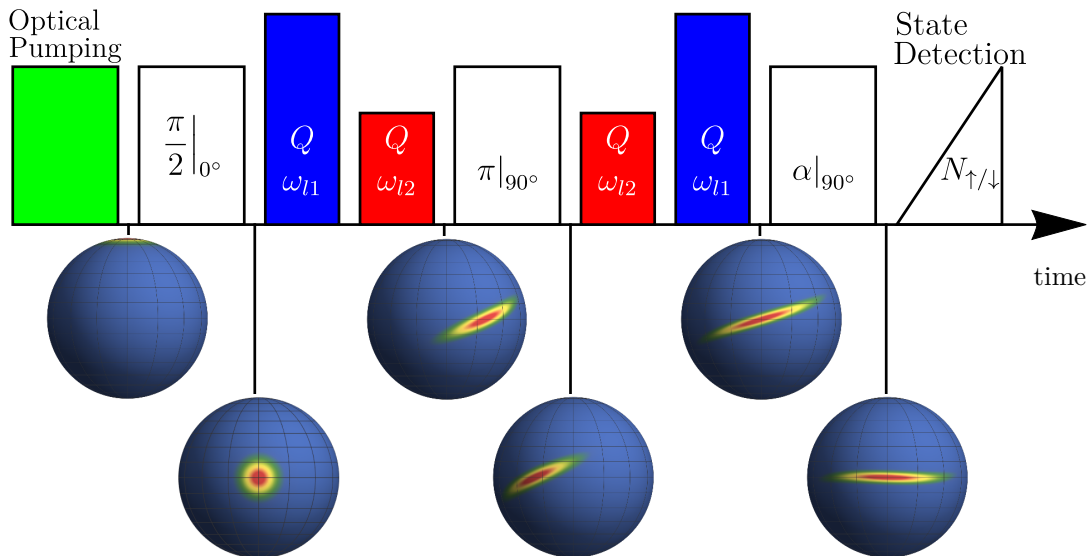
FIG. S4: Full experimental sequence for spin squeezing. The subscript in the RF pulses indicates the axis of the rotation. The spheres below the sequence indicate the collective spin state at the corresponding time.

probing pulses detuned from the atomic frequency by more than the Rabi splitting ($|\omega_l - \omega_a| > g \approx 2\pi \times 4\,\text{MHz}$) will introduce a larger shearing per incident photon; conversely, pulses with $|\omega_l - \omega_a| < g$ will induce less shearing. Thus, by sending two separate probing pulses with appropriately chosen frequencies and relative intensities, it is possible to avoid broadening of the generated squeezed state due to fluctuations in N.

To achieve first-order insensitivity to atom number fluctuations around $N\eta = 1800$ with $\eta = 1.8$, we choose the parameters $((\omega_{l1} - \omega_a)/(2\pi) = 7.33\,\text{MHz}$, $(\omega_{l2} - \omega_a)/(2\pi) = -2\,\text{MHz}$, and incoming power ratio $P_2/P_1 = 0.53$. For the conditions in which we obtained the results reported in the main text, the model predicts, a maximum variation of Q equal to 8% in the range $1600 < N\eta < 2000$. Fig. S5 shows a measurement of the compensation together with a prediction from the theoretical model (see Sec. VII) with no free parameters.
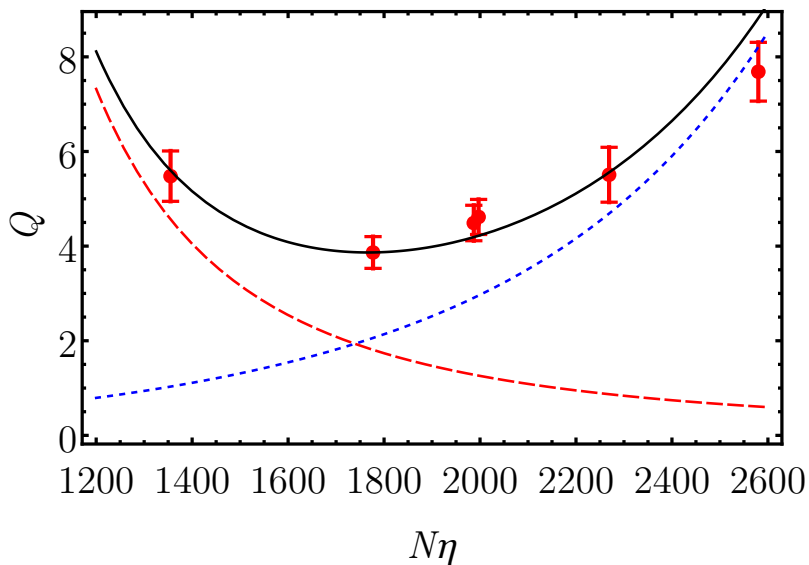

FIG. S5: Compensation for total atom number fluctuations measured for $\omega_{l1} = 7.334\,\text{MHz}$ and $\omega_{l2} = -2.5\,\text{MHz}$, $\eta = 3$. Note that these measurements were taken at slightly different conditions than the other results in the main text. The two squeezing pulses have power ratio $P_2/P_1 = 0.53$. Blue dotted, red dashed and black solid lines stand for theoretical calculation for shearing strength Q due to the ω_{l1} pulse, the ω_{l2} pulse and both together, respectively, while the red circles indicate experimental results. Around $N\eta \approx 1800$, Q depends only weakly on the total atom number.

VII. THEORETICAL MODEL FOR SQUEEZING AND MEASUREMENT STRENGTH

The squeezing is caused by light circulating in the cavity that is influenced by the quantum noise of the atomic spin S_z [7, 17]. For $\omega_l, \omega_c, \omega_a$ being the angular frequencies of the incident light, the empty cavity, and the atomic transition, respectively, we define normalized cavity and atomic detuning $x = 2(\omega_l - \omega_c)/\kappa$, $y = 2(\omega_l - \omega_a)/\Gamma$, and

$$\mathcal{L}_a(y) = \frac{1}{1 + y^2} \tag{S4}$$

$$\mathcal{L}_d(y) = -\frac{y}{1 + y^2} \tag{S5}$$

as the absorptive and dispersive Lorentzian lineshapes, respectively. Then in the two-level approximation, where only the state $|\uparrow\rangle$ is coupled to an excited state, the Hamiltonian of the system can be written as [14, 18]

$$H = S_z \eta \frac{|\mathcal{E}_c|^2}{\omega_l} \frac{\pi}{\mathcal{F}} \mathcal{L}_d(y) \tag{S6}$$

Here, $\mathcal{E}_c$ is the amplitude of the circulating intracavity electric field. This Hamiltonian causes a precession of the spin that is canceled by the spin echo π pulse (see Sec. V and Fig. S4). Furthermore, due to the dependence of the cavity field $\mathcal{E}_c$ on S_z, different S_z components experience different phase shifts (one-axis twisting [19]). The shearing strength Q is defined as the second derivative of the phase shift with respect to S_z. Expressing Q by the transmitted photon number p_{tr} for a (nearly) one-sided cavity driven through the low-transmission mirror, we obtain for the shearing strength $\hat{Q}$ per transmitted photon the following expression:

$$\hat{Q}_{tr} \equiv \frac{Q}{p_{tr}} = -\frac{y}{2(1 + y^2)^2} \frac{N_\uparrow \eta^2 (1 + N_\uparrow \eta - xy)}{(1 + N_\uparrow \eta \mathcal{L}_a(y))^2 + (x + N_\uparrow \eta \mathcal{L}_d(y))^2}. \tag{S7}$$

Since at fixed parameters the photon number scattered by the atoms into free space is proportional to the transmitted photon number p_{sc}, we can easily find the shearing strength $\hat{Q}_{sc} = Q/p_{sc}$ per scattered photon. For our parameters we calculate $\hat{Q}_{sc}^{(1)} = 0.014, \hat{Q}_{sc}^{(2)} = 0.097$ for the blue and red detuned probing pulses, respectively. Taking the input intensity ratio $P_2/P_1 = 0.53$ and the cavity transmission ratio $T_2/T_1 = 0.27$ into account, the average shearing strength per scattered photon is $\hat{Q}_{sc} = 0.024$.

The excess state broadening F over unitary squeezing arises from the fact that the transmitted and scattered light carries some residual information about the atomic spin S_z, and tracing over the light degrees of freedom causes excess antisqueezing of the atomic spin. We define $1 + F$ as the factor by which the minimum spin quadrature variance is increased due to excess antisqueezing. It can be shown that F is proportional to the transmitted or scattered photon number. The value $\hat{F}$ per transmitted photon is calculated as [14, 18, 20]:

$$\hat{F}_{tr} \equiv \frac{F}{p_{tr}} = \frac{2}{(1 + y^2)^2} \frac{N_\uparrow \eta^2 (1 + N_\uparrow \eta + y^2)}{(1 + N_\uparrow \eta \mathcal{L}_a(y))^2 + (x + N_\uparrow \eta \mathcal{L}_d(y))^2}. \tag{S8}$$

This gives for the excess broadening per scattered photon $\hat{F}_{sc}^1 = 0.0018$ and $\hat{F}_{sc}^2 = 0.016$. Taking the intensity ratio into account, we have $\hat{F}_{sc} = 0.0036$ per scattered photon.

VIII. EFFECT OF BLOCH SPHERE CURVATURE

To lowest order in Q, the one-axis twisting Hamiltonian simply induces unitary squeezing with quadrature variances given by Eq. (2). However, due to the curvature of the Bloch sphere, the minimum spin quadrature increases [19], with the next-lowest order term being an increase of the minimum spin quadrature variance by $Q^4/(24S^2)$ for a homogeneously coupled system [21]. In our inhomogeneously coupled system, this curvature-induced broadening is twice as large: $Q^4/(12S^2)$. This term reproduces the observed broadening at $Q \gtrsim 10$ in Fig. 3 in the main text. The Bloch sphere curvature limits the maximum squeezing to $\xi_-^2 \geq -15.8$ dB.

IX. CAVITY QED PARAMETERS USED IN THIS EXPERIMENT

The cavity and atomic parameters are summarized in Table I. For more details regarding the cavity see Ref. [2]. Some parameters have changed their values due to aging of the experimental setup and are slightly different from those summarized in Table I of Ref. [2]. Note that the cavity linewidth κ includes broadening from the relative frequency stability of the cavity and 556 nm probe laser, while the cavity finesse $\mathcal{F}$ is obtained via a ringdown measurement which is sensitive to the properties of the cavity alone. The total detection efficiency ϵ for a photon initially inside the cavity includes mirror losses, detection path loss, and finite photodetector quantum efficiency.

Atomic wavelength	$\lambda = 555.799$ nm
Atomic linewidth of $^3P_1$ state	$\Gamma/(2\pi) = 184(1)$ kHz
Cavity linewidth	$\kappa/(2\pi) = 520(15)$ kHz
Cavity finesse	$\mathcal{F} = 12.2(4) \times 10^3$
Transmission of $R_1 = 25$ mm mirror	30(1) ppm
Transmission of $R_2 = 344\,\mu$m mirror	196(5) ppm
Cavity detuning	$(\omega_c - \omega_a)/(2\pi) = -340(10)$ kHz
Effective cooperativity	$\eta = 1.8(1)$
Atomic temperature	$T = 20(5)\,\mu$K
Lattice depth	$U_0/h = 2.5(6)$ MHz
Axial trapping frequency	$\omega_{ax}/(2\pi) = 140(4)$ kHz
Radial trapping frequency	$\omega_r/(2\pi) = 1.4(1)$ kHz
Total photon detection efficiency	$\epsilon = 15(1)\%$

TABLE I: Summary of most relevant parameters used in this experiment.

X. STATISTICAL AND SYSTEMATIC ERRORS

A. Statistical errors

The statistical error in the variance estimation with n measurements is given by

$$\Delta\sigma^2 = \sigma^2 \sqrt{\frac{2}{n-1}}. \tag{S9}$$

Each σ_α^2 in the tomography (see Fig. 2 in the main text) is obtained by collecting more than 100 measurements, resulting in fractional uncertainties smaller than 12%. For each state tomography curve we performed more than 1000 experiments; we used the whole set of data to estimate the state readout σ_d^2, resulting thus in a fractional uncertainty smaller than 5%.

B. Systematic errors

From day to day we observe fluctuations in the estimated state readout σ_d^2. We attribute this to systematic variations of the 556 nm laser frequency on the order of ± 40 kHz. This induces changes in the contrast of the beat note produced in the heterodyne measurement of S_z (see Section II), resulting in fluctuating efficiency of the information derived from the phase of the beatnote at $2\omega_m$ (see Fig. S2).

Thus, the σ_d^2=9.4(4) dB as specified in the main text is dominated by this systematic error.

C. Extra considerations on errorbars

The experiment for each shearing strength Q was performed on a different day. To infer the spin projection noise and the potential metrological gain, we use the measurement resolution σ_d^2 obtained on that particular day. In this case the σ_d^2 is not affected by daily variations and its uncertainty is only statistical. Each day the measurement resolution

is obtained from $\geq$1000 data, resulting in a fractional uncertainty $\leq$4.5%. Each ξ_{st}^2 and ξ_W^2 without readout noise are derived by subtracting the daily value of σ_d^2 from the measured spin projection noise reduction ξ_-^2. The errorbars of the inferred spin projection noise ξ_{st}^2 (see Fig. 4(a) in main text) are obtained by combining this uncertainty with those of Q and F obtained from the tomography measurements (see Fig. 2 in main text). Finally, the maximal spin projection noise and potential metrological gain are obtained from the minimum of the ξ_{st}^2 measured curve. The resulting values of ξ_{st}^2=15.9(6) dB and ξ_W^2=12.9(6) dB have uncertainties smaller than the single-measurement uncertainty.

[1] A. Kawasaki, B. Braverman, Q. Yu, and V. Vuletić, J. Phys. B **48**, 155302 (2015), ISSN 0953-4075, URL http://stacks.iop.org/0953-4075/48/i=15/a=155302.

[2] A. Kawasaki, B. Braverman, E. Pedrozo-Peñafiel, C. Shu, S. Colombo, Z. Li, O. Özel, W. Chen, L. Salvi, A. Heinz, et al., Phys. Rev. A **99**, 013437 (2019), URL https://link.aps.org/doi/10.1103/PhysRevA.99.013437.

[3] H. Tanji-Suzuki, I. D. Leroux, M. H. Schleier-Smith, M. Cetina, A. T. Grier, J. Simon, and V. Vuletić, in *Advances in Atomic, Molecular, and Optical Physics*, edited by P. B. E. Arimondo and C. Lin (Academic Press, 2011), vol. 60, pp. 201 – 237, URL http://www.sciencedirect.com/science/article/pii/B9780123855084000048.

[4] M. G. Raizen, R. J. Thompson, R. J. Brecha, H. J. Kimble, and H. J. Carmichael, Phys. Rev. Lett. **63**, 240 (1989), URL https://link.aps.org/doi/10.1103/PhysRevLett.63.240.

[5] P. Münstermann, T. Fischer, P. Maunz, P. W. H. Pinkse, and G. Rempe, Phys. Rev. Lett. **82**, 3791 (1999), URL https://link.aps.org/doi/10.1103/PhysRevLett.82.3791.

[6] E. J. Davis, G. Bentsen, L. Homeier, T. Li, and M. H. Schleier-Smith, Phys. Rev. Lett. **122**, 010405 (2019), URL https://link.aps.org/doi/10.1103/PhysRevLett.122.010405.

[7] M. H. Schleier-Smith, I. D. Leroux, and V. Vuletić, Phys. Rev. Lett. **104**, 073604 (2010), URL http://link.aps.org/doi/10.1103/PhysRevLett.104.073604.

[8] J. Hu, W. Chen, Z. Vendeiro, H. Zhang, and V. Vuletić, Phys. Rev. A **92**, 063816 (2015), URL https://link.aps.org/doi/10.1103/PhysRevA.92.063816.

[9] M. H. Schleier-Smith, I. D. Leroux, and V. Vuletić, Phys. Rev. A **81**, 021804(R) (2010), URL http://link.aps.org/doi/10.1103/PhysRevA.81.021804.

[10] O. Hosten, N. J. Engelsen, R. Krishnakumar, and M. A. Kasevich, Nature (London) **529**, 505 (2016), ISSN 0028-0836, URL http://dx.doi.org/10.1038/nature16176.

[11] K. C. Cox, G. P. Greve, J. M. Weiner, and J. K. Thompson, Phys. Rev. Lett. **116**, 093602 (2016), URL https://link.aps.org/doi/10.1103/PhysRevLett.116.093602.

[12] M. Saffman, D. Oblak, J. Appel, and E. S. Polzik, Phys. Rev. A **79**, 023831 (2009), URL http://link.aps.org/doi/10.1103/PhysRevA.79.023831.

[13] Z. Chen, J. G. Bohnet, J. M. Weiner, K. C. Cox, and J. K. Thompson, Phys. Rev. A **89**, 043837 (2014), URL http://link.aps.org/doi/10.1103/PhysRevA.89.043837.

[14] B. Braverman, Ph.D. thesis, Massachusetts Institute of Technology (2018).

[15] H. K. Cummins, G. Llewellyn, and J. A. Jones, Phys. Rev. A **67**, 042308 (2003), URL https://link.aps.org/doi/10.1103/PhysRevA.67.042308.

[16] M. Bando, T. Ichikawa, Y. Kondo, and M. Nakahara, J. Phys. Soc. Jpn. **82**, 014004 (2013), URL https://doi.org/10.7566/JPSJ.82.014004.

[17] I. D. Leroux, M. H. Schleier-Smith, and V. Vuletić, Phys. Rev. Lett. **104**, 073602 (2010), URL http://journals.aps.org/prl/abstract/10.1103/PhysRevLett.104.073602.

[18] B. Braverman, A. Kawasaki, E. Pedrozo-Peñafiel, C. Shu, S. Colombo, Z. Li, and V. Vuletić (2019), manuscript in preparation.

[19] M. Kitagawa and M. Ueda, Phys. Rev. A **47**, 5138 (1993), URL http://link.aps.org/doi/10.1103/PhysRevA.47.5138.

[20] A. Kawasaki, Ph.D. thesis, Massachusetts Institute of Technology (2017).

[21] I. D. Leroux, M. H. Schleier-Smith, H. Zhang, and V. Vuletić, Physical Review A **85**, 013803 (2012).